Polζ ablation in B cells impairs the germinal center reaction, class switch recombination, DNA break repair, and genome stability

Dominik Schenten,[1,2] Sven Kracker,[1,2] Gloria Esposito,[3] Sonia Franco,[1,2,4] Ulf Klein,[3] Michael Murphy,[1] Frederick W. Alt,[1,2,4,5] and Klaus Rajewsky[1,2,3]

[1]Immune Disease Institute, Boston, MA 02115
[2]Harvard Medical School, Boston, MA 02115
[3]Institute for Genetics, University of Cologne, D-50674 Cologne, Germany
[4]The Children's Hospital, Boston, MA 02115
[5]Howard Hughes Medical Institute, Chevy Chase, MD 20815

Polζ is an error-prone DNA polymerase that is critical for embryonic development and maintenance of genome stability. To analyze its suggested role in somatic hypermutation (SHM) and possible contribution to DNA double-strand break (DSB) repair in class switch recombination (CSR), we ablated Rev3, the catalytic subunit of Polζ, selectively in mature B cells in vivo. The frequency of somatic mutation was reduced in the mutant cells but the pattern of SHM was unaffected. Rev3-deficient B cells also exhibited pronounced chromosomal instability and impaired proliferation capacity. Although the data thus argue against a direct role of Polζ in SHM, Polζ deficiency directly interfered with CSR in that activated Rev3-deficient B cells exhibited a reduced efficiency of CSR and an increased frequency of DNA breaks in the immunoglobulin H locus. Based on our results, we suggest a nonredundant role of Polζ in DNA DSB repair through nonhomologous end joining.

CORRESPONDENCE
Klaus Rajewsky:
rajewsky@idi.med.harvard.edu

Abbreviations used: AID, activation-induced deaminase; CSR, class switch recombination; DSB, double-strand break; ES, embryonic stem; FISH, fluorescence in situ hybridization; GC, germinal center; NHEJ, nonhomologous end joining; SHM, somatic hypermutation; SKY, spectral karyotyping; V, variable.

In T cell–dependent antibody responses, B cells are triggered to undergo a second round of antibody diversification in germinal centers (GCs) (1). Somatic hypermutation (SHM) introduces mutations into rearranged variable (V) regions of Ig genes allowing antibody affinity maturation (2, 3), whereas class switch recombination (CSR) exchanges the Ig constant (C) region to modify the effector function of the antibody (4). Both SHM and CSR rely on activation-induced deaminase (AID), an enzyme which deaminates cytidine residues in single-stranded DNA (5). The DNA deamination model of SHM suggests the conversion of G-C basepairs into G-U mismatches within the V region by AID (6, 7), which are subsequently processed in one of three ways: direct replication across the G-U mismatches results in G-C to A-T mutations; the removal of the uracil residues by the uracil deglycosylase UNG creates abasic sites, and DNA synthesis by error-prone DNA polymerases generates additional mutations; or the recognition of the G-U mismatches by the mismatch repair enzymes MSH2 and MSH6 leads to subsequent error-prone short-patch DNA synthesis, which introduces mutations outside the initial site of the lesion.

In the case of CSR, it is widely believed that upon cytidine deamination by AID, staggered DNA double-strand breaks (DSBs) are generated by the removal of the uracil residues by UNG, followed by the cleavage of the abasic sites by APE1/2 during the G1 phase of the cell cycle (5, 8–13). Alternatively, the mismatch–repair pathway can lead to the generation of staggered DSBs via the recognition of uracil by

D. Schenten, S. Kracker, and G. Esposito contributed equally to this paper.

D. Schenten's present address is Dept. of Immunobiology, Yale Medical School, New Haven, CT 06520.

G. Esposito's present address is TaconicArtemis, 51063 Cologne, Germany.

U. Klein's present address is Institute for Cancer Genetics and Herbert Irving Comprehensive Cancer Center, Columbia University, New York, NY 10032.

The Rockefeller University Press $30.00
J. Exp. Med. Vol. 206 No. 2 477-490
www.jem.org/cgi/doi/10.1084/jem.20080669

MSH2 and MSH6 (8, 14, 15). The DSBs are then resolved by a process that includes DNA damage response proteins such as H2AX, MDC1, ATM, 53BP1, and the Nibrin–Mre11–Rad50 complex, the mismatch repair enzymes Pms2 and Mlh1, the exonuclease Exo1, and the classical and alternative nonhomologous end-joining (NHEJ) machinery (16–28).

Although the DNA polymerases required for filling in the staggered DNA breaks generated in CSR have not been identified, a possible involvement of several error-prone DNA polymerases in SHM has been tested using both hypermutating cell lines and KO mice deficient of these enzymes. From this work, Polη, Polθ, and perhaps Polι have emerged as important components of the SHM mechanism, whereas Polβ, Polκ, Polλ, and Polμ do not appear to play a significant role (29–35). Polζ is an error-prone DNA polymerase that is characterized by its ability to extend mismatched primer-template termini (36). Polζ, together with Polι, has been suggested as the prime example of the two-step inserter-extender model of translesion synthesis, in which a first DNA polymerase (Polι) synthesizes across the DNA lesion and a second polymerase (Polζ) extends the resulting mismatch (36). These features highlighted Polζ as an additional candidate enzyme of the SHM machinery. Indeed, studies in a hypermutating cell line and a transgenic mouse strain that express antisense RNA against Rev3, the catalytic subunit of Polζ, demonstrated a reduction of the frequency of somatic mutations in rearranged Ig V region genes, suggesting an involvement of Polζ in SHM (37, 38).

Attempts to address this issue in vivo by genetically ablating Polζ in mice have been hampered by the embryonic lethality observed upon deletion of the Polζ gene in the mouse germ line (39–41). This embryonic lethality could be a result of the pronounced genomic instability observed upon Polζ ablation in a wide variety of cellular systems (42), in turn suggesting a role of this enzyme in DNA repair and thus, potentially, CSR (16). To assess a possible contribution of Polζ to SHM and CSR in vivo, we generated mice that carry a deletion of Rev3 selectively in mature B cells (subsequently called *Polζ$^{f/Δ}$/CD21-cre* mice). In this paper, we show that Polζ-deficient B cells are impaired in their ability to proliferate and to maintain a stable genome. The mutant cells fail to undergo an efficient GC reaction and exhibit a reduced frequency of SHM and impaired CSR. The CSR defect is associated with an increased frequency of aberrantly or unrepaired DNA breaks within the IgH locus, suggesting that Polζ plays a nonredundant role in DNA DSB repair through NHEJ.

RESULTS

Generation of a conditional *Polζ* allele

This was achieved by flanking exon 2 of the *Rev3* gene by loxP sites, to allow its deletion by Cre-mediated recombination (Fig. 1, A and B). Exon 2 is the second coding exon of *Rev3*, and messenger RNA splicing from exon 1 to exon 3 results in a frameshift mutation. Some *Rev3* transcripts incorporate an additional exon downstream of exon 1. RNA splicing from this exon to exon 3 also results in a frameshift mutation (43). Two targeted embryonic stem (ES) cell clones were injected into blastocysts. Mice carrying the floxed *Rev3* allele (subsequently called *Polζ^{f}*) were viable and born at Mendelian ratios. The correct targeting of the *Rev3* locus was confirmed by a nested PCR assay on tail DNA from *Polζ$^{f/+}$* mice and wild-type controls. The PCR relied on a forward primer located outside the targeting vector to ensure the integration of the latter into the *Rev3* locus, and a reverse primer located 3′ of the downstream loxP site. The amplicons of both the wild-type and floxed alleles migrated at the expected size of ∼5.2 kb (unpublished data). The PCR products were then gel purified and used as templates for two separate PCRs that amplified across the first and second loxP site, respectively. Each PCR amplified only one band for wild-type mice. In *Polζ$^{f/+}$* mice, however, an additional band appeared in both cases whose larger size was consistent with the presence of an inserted loxP site (Fig. 1 C). Mice carrying the *Polζ^{f}* allele were intercrossed with *CD21-cre* or *deleter* mice to generate *Polζ$^{f/Δ}$/CD21-cre* compound mutants, in which Polζ function was specifically inactivated in mature B cells (44, 45). The deletion of exon 2 in the *Polζ^{Δ}* allele was confirmed by gene amplification and subsequent sequencing of the PCR product (unpublished data).

Immune response and GC formation in *Polζ$^{f/Δ}$/CD21-cre* mice

No defects in B cell development were observed in *Polζ$^{f/Δ}$/CD21-cre* mice (unpublished data). Likewise, the number and proportions of resting B cells in the periphery was indistinguishable from those in control mice (unpublished data). We then characterized the antibody response of *Polζ$^{f/Δ}$/CD21-cre* mice against the T cell–dependent antigen NP-CG (3-hydroxy-nitrophenyl acetyl coupled to chicken γ-globulin). We injected *Polζ$^{f/Δ}$/CD21-cre* mice and control animals with 100 μg NP-CG in alum intraperitoneally and measured the serum titers of the NP-specific IgG1 and Igλ antibodies at days 7 and 14 after immunization. At both time points, the response of *Polζ$^{f/Δ}$/CD21-cre* mice was reduced by 50% compared with that of control mice (unpublished data). Polζ deficiency may affect cell viability of highly proliferating cells such as GC B cells. We therefore compared the proportions of CD19^{+}Fas^{+}PNA^{high} GC B cells in spleen, mesenteric lymph nodes, and Peyer's patches of *Polζ$^{f/Δ}$/CD21-cre* and control mice that had been immunized with 100 μg NP-CG in alum 14 d earlier. The GC B cell compartment of *Polζ$^{f/Δ}$/CD21-cre* mice was 2–3-fold smaller than that in control animals (Fig. 2 A), suggesting an impairment of cell proliferation or cell viability in the absence of Polζ. To test whether this resulted in an accumulation of B cells that had escaped Cre-mediated inactivation of *Polζ*, we isolated CD19^{+}Fas^{+}PNA^{high} GC B cells and CD19^{+}Fas^{-}PNA^{low} naive B cells from *Polζ$^{f/Δ}$/CD21-cre* mice and control mice 14 d after immunization by flow cytometry and determined the deletion efficiency of the *Polζ^{f}* allele in these cells by PCR. Competitive amplification of the *Polζ^{f}* and *Polζ^{Δ}* alleles and comparison to a standard curve with known ratios of the two alleles showed that ∼90% of the PCR products in the CD19^{+}Fas^{-}PNA^{low} B cell

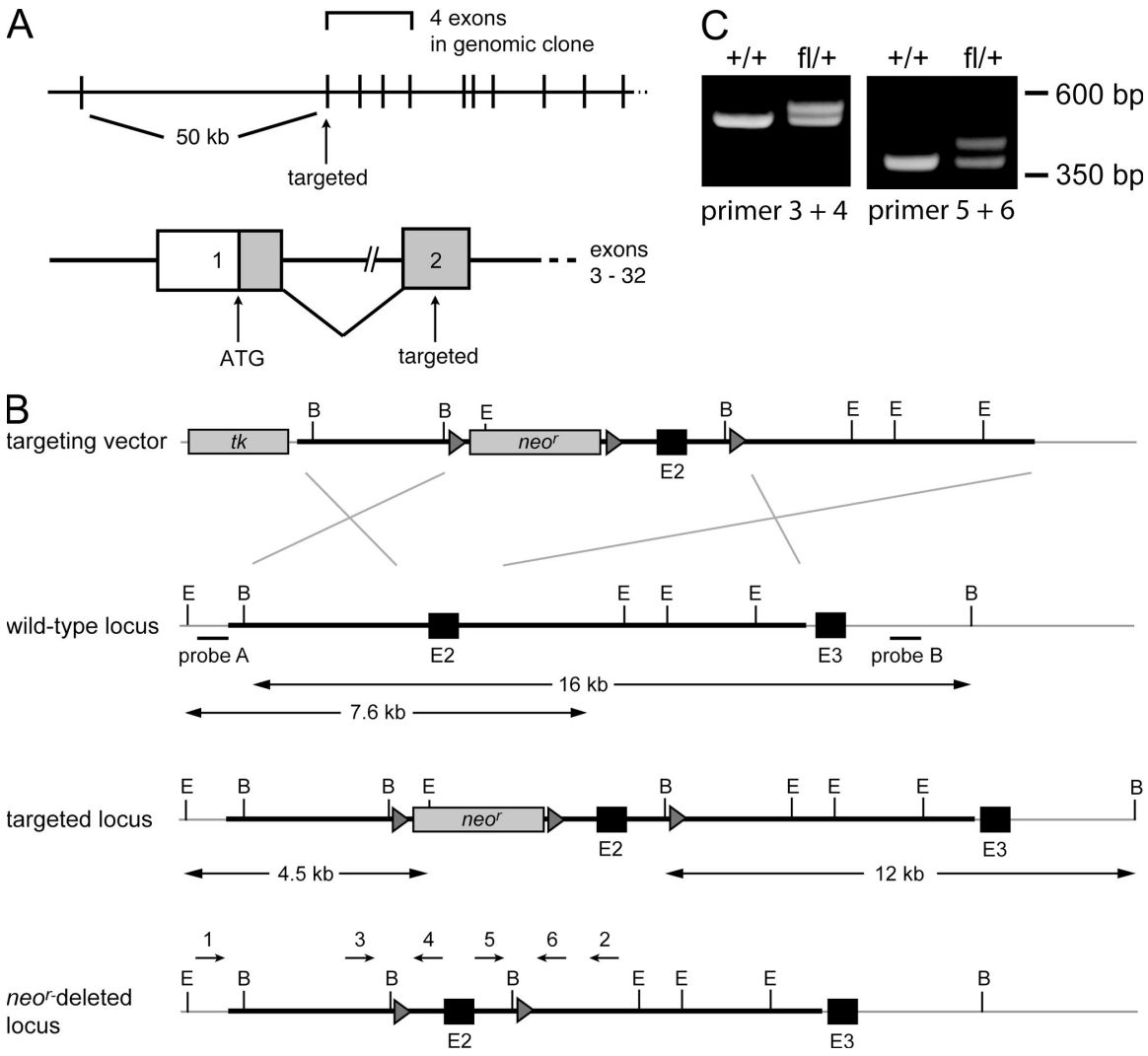

Figure 1. Conditional inactivation of *Polζ*. (A) Schematic representation of the Rev3 locus and gene structure at the 5′ end. Vertical lines or boxes represent exons. The shaded areas indicate coding regions. The map is not drawn to scale. (B) Schematic representation of the gene targeting strategy. Bold lines, regions of homology; black boxes, exons; gray boxes, selection markers; tk, thymidine kinase gene; neo^r, neomycin resistance gene; triangles, loxP sites; B, BamHI sites; E, EcoRI sites. The predicted sizes of DNA fragments detected by Southern blot hybridization with probe A or probe B on EcoRI and BamHI-digested genomic DNA, respectively, as well as the location of the primers polz-1 to polz-6 for the genomic PCRs (short arrows) are indicated. The map is not drawn to scale. (C) Analysis of the targeted *rev3* locus. The wild-type and targeted alleles were distinguished by nested PCRs on tail DNA from *Polζ*$^{+/f}$ and wild-type mice. The first PCR round relied on primers 1 and 2 that anneal 5′ of the region of homology and 3′ of the second loxP site, respectively. This was followed by an amplification step of the gel-purified PCR product using the primer pairs 3 and 4 or 5 and 6, which flank the first and second loxP site, respectively. For primer pair 3 and 4, the expected sizes of the wild-type and targeted PCR products are 523 and 583 bp. For primer pair 5 and 6, the expected sizes are 384 and 458 bp.

fraction and 80% in the CD19$^+$Fas$^+$PNA^{high} B cell fraction were derived from the *Polζ*^{Δ} allele in *Polζ*$^{f/Δ}$*/CD21-cre* mice (Fig. 2 B). This corresponds to a deletion efficiency of 80% in naive and 60% in GC B cells, as the mice were heterozygous for the *Polζ*^{Δ} allele. Thus, there was a moderate enrichment of cells that failed to inactivate Polζ in the GCs.

Reduced mutation frequency in *Polζ*$^{f/Δ}$*/CD21-cre* mice

To examine the impact of Polζ deficiency on SHM, we isolated naive and GC B cells from *Polζ*$^{f/Δ}$*/CD21-cre* and control mice that had been immunized with NP-CG 14 d earlier. As in the mutants, a substantial fraction of these cells had escaped Cre-mediated recombination. An analysis of VDJ joints amplified from populations of such cells is a priori compromised. Indeed, when we analyzed the accumulation of somatic mutations by bulk PCR using a primer pair that anneals in the framework region 3 of most V_HJ558 gene segments and in the intron downstream of the J_H4 gene segment (46), we found only a moderate reduction of the frequency of SHM in the mutants compared with the controls (Fig. S1 A, available at http://www.jem.org/cgi/content/full/jem.20080669/DC1). 76 and 79% of the mutations in *Polζ*$^{f/Δ}$*/CD21-cre* mice occurred at

A-T basepairs, compared with 56 and 65% in the controls. There was no difference in the ratio of transitions to transversions between mutants and controls (Fig. S1 B).

To approach the impact of Polζ deficiency on SHM at a higher level of resolution, we analyzed the accumulation of somatic mutations in *Polζ*$^{f/\Delta}$*/CD21-cre* mice at the level of single GC B cells, which we simultaneously genotyped for the inactivation of the *Polζ* gene. This approach offered an additional advantage in that it is not sensitive to a different rate of PCR errors across the individual samples. We isolated single GC B cells by flow cytometry and performed a PCR using a primer pair that anneals in the framework region 3 of most V_HJ558 gene segments and in the intron downstream of the J_H4 gene segment together with primer pairs that allow the genotyping of the *Polζ*^{f} and *Polζ*$^\Delta$ alleles. The amplification efficiency of both the *Polζ*^{f} and the *Polζ*$^\Delta$ allele in sorted GC *Polζ*$^{f/\Delta}$ B cells was 80%. We successfully amplified the rearranged J_H gene segments in 66% of *Polζ*$^{f/\Delta}$ GC B cells from mice without the *CD21-cre* allele, in 42% of *Polζ*$^{f/\Delta}$ GC B cells from *Polζ*$^{f/\Delta}$*/CD21-cre* mice, and in 66% of *Polζ*$^{\Delta/\Delta}$ GC B cells from *Polζ*$^{f/\Delta}$*/CD21-cre* mice. These differences in amplification efficiencies likely resulted from different extents of contamination of the sorted cells by non-B cells. The PCR products corresponding to the four introns downstream of the rearranged J_H gene segments were sequenced and analyzed for the presence of somatic mutations. GC B cells that had ablated Polζ mutated

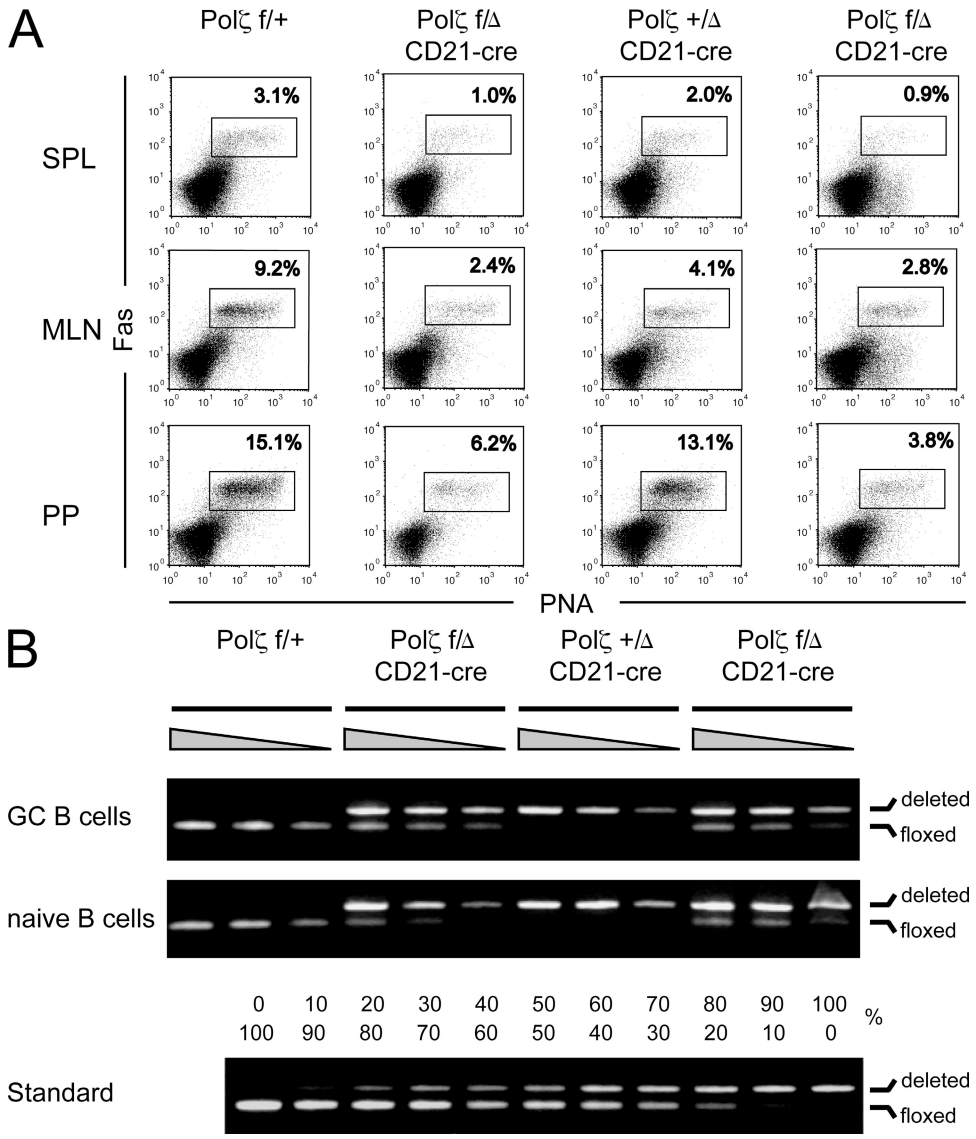

Figure 2. GC formation in *Polζ*$^{f/\Delta}$*/CD21-cre* mice. (A) Generation of GC B cells. Mice were immunized with 100 µg NP-CG in alum and analyzed for the presence of CD19$^+$PNA$^+$Fas$^+$ GC B cells 14 d after immunization. Only CD19$^+$ cells are shown. SPL, spleen; PP, Peyer's patches; MLN, mesenteric lymph nodes. Data represent one of two independent experiments. (B) Deletion efficiency of the *Polζ*^{f} allele. The *Polζ*^{f} and *Polζ*$^\Delta$ alleles in B cells of *Polζ*$^{f/\Delta}$*/CD21-cre* and control mice were amplified in a competitive PCR using primers that anneal 5′, within, and 3′ of the floxed region and compared with a standard with known ratios of the two alleles. The fragments corresponding to the floxed and deleted allele migrate at around 300 and 450 bp, respectively.

their Ig genes with a frequency of 0.19% (Fig. 3 A). In contrast, the mutation frequency in GC B cells that had retained the *Polζ*^{f} allele was 0.68%. Moreover, almost 50% of all sequences derived from *Polζ*$^{\Delta/\Delta}$ cells contained only one mutation, whereas close to 80% of the sequences derived from *Polζ*$^{f/\Delta}$ cells had multiple mutations. Likewise, 38% of the sequences derived from *Polζ*$^{\Delta/\Delta}$ cells remained unmutated.

To compare the pattern of somatic mutations in mutants and controls, we first established the mutation patterns in the individual introns downstream of each rearranged J_H gene segment. Subsequently, we normalized the mutation patterns to the base composition of the respective intron and then combined the mutation patterns of all four introns. There was no significant difference in the mutation pattern between

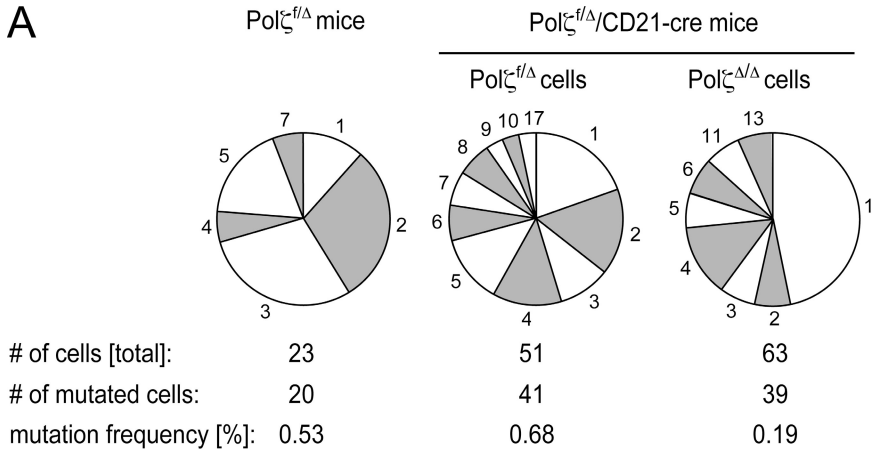

B

Polζ$^{f/\Delta}$ mice

n = 86	to A	G	C	T	Sum	Tr./Tv.
from A	–	19	12	9	40	1.0
from G	16	–	11	2	30	
from C	4	1	–	12	17	
from T	9	0	4	–	13	

Polζ$^{f/\Delta}$/CD21-cre mice

Polζ$^{f/\Delta}$ cells

n = 199	to A	G	C	T		Tr./Tv.
from A	–	25	6	16	47	1.3
from G	13	–	6	4	23	
from C	3	2	–	11	16	
from T	3	3	9	–	15	

Polζ$^{\Delta/\Delta}$ cells

n = 81	to A	G	C	T		Tr./Tv.
from A	–	22	6	20	47	1.1
from G	14	–	2	5	21	
from C	2	6	–	9	17	
from T	7	1	7	–	15	

C

	Polζ$^{f/\Delta}$ mice	Polζ$^{f/\Delta}$/CD21-cre mice	
		Polζ$^{f/\Delta}$ cells	Polζ$^{\Delta/\Delta}$ cells
A/T	53 %	61 %	62 %
G/C	47 %	39 %	38 %

Figure 3. Single cell analysis of SHM in *Polζ*$^{f/\Delta}$*/CD21-cre* mice. (A) Distribution of mutations per B cell and mutation frequency in *Polζ*-deficient and *Polζ*-proficient B cells. Single GC B cells were sorted by FACS 14 d after immunization with NP-CG. PCR fragments containing the introns downstream of the rearranged V(D)J elements were amplified in a seminested PCR and subsequently sequenced. Simultaneously, the single cells were genotyped for the presence of the *Polζ*^{f} allele. The mutation frequency was determined by the number of mutations present in the sequence of 500 bp, downstream of the individual VDJ rearrangement. (B) To compare the patterns of mutations of Polζ-deficient and -proficient cells, sequences derived from B cells using the same rearranged J_H element were grouped together and the mutations in each group were counted. The emerging mutation pattern in each group was corrected for the base composition of that particular intron before the patterns of the four J_H introns were compiled together. All values are shown in percentages and were rounded to the nearest whole number. *n* = the number of mutations; Tr./Tv., the transitions (Tr.) over transversions (Tv.) ratio. Shown are the combined mutation patterns corrected for the base composition of the sequences. (C) Percentage of mutations at A-T versus C-G basepairs in the same analysis.

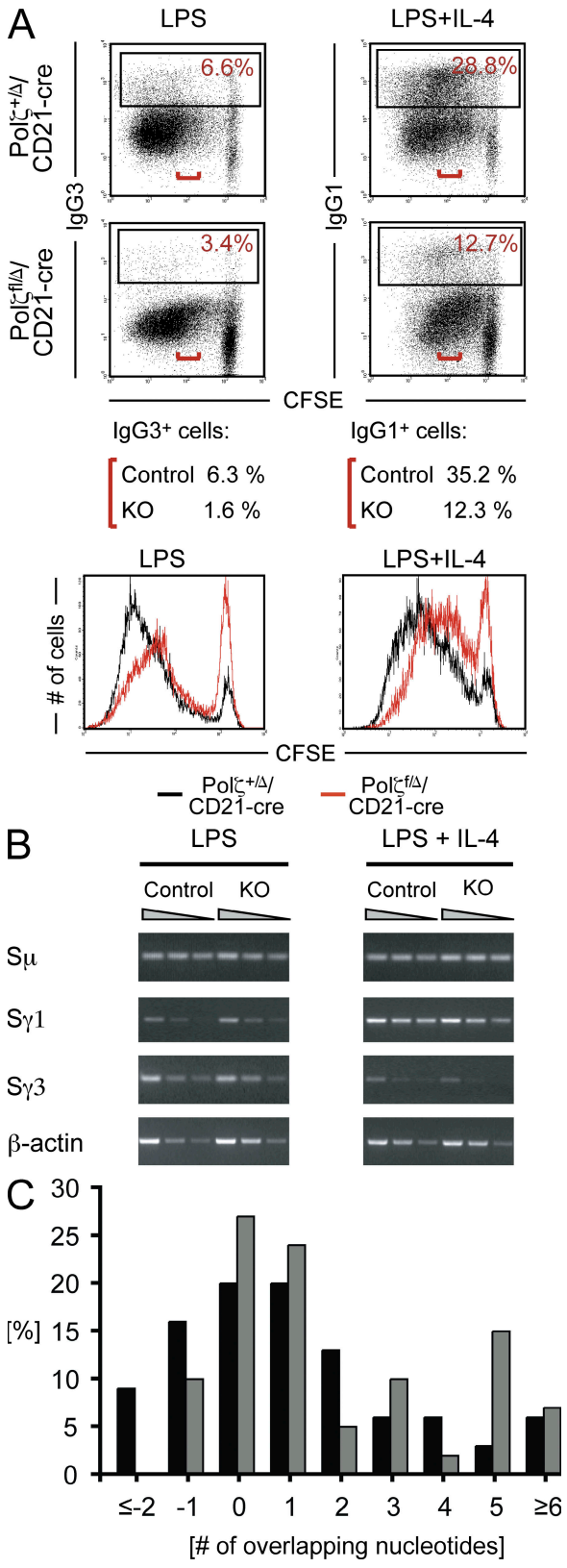

Figure 4. CSR in *Polζ$^{f/Δ}$/CD21-cre* B cells. (A) In vitro stimulation of isolated B cells of *Polζ$^{f/Δ}$/CD21-cre* and control mice. B cells were induced to undergo CSR with either LPS and IL-4 or LPS alone. The percentage of class-switched cells was determined 4 d later by flow cytometry. Numbers in the graphs represent the percentage of switched cells. Numbers next to the red brackets below the graphs represent the percentage of class-switched cells among cells that have proliferated similarly, as indicated by the red brackets in the graphs. The histograms depict the proliferation of all cells in the culture. Black lines, *Polζ$^{+/Δ}$/CD21-cre* cells; red lines, *Polζ$^{f/Δ}$/CD21-cre* cells. Data represent one of three independent experiments. (B) Germline transcription of the S regions in *Polζ$^{f/Δ}$/CD21-cre* mice and control mice. B cells were stimulated with LPS or LPS + IL-4 to undergo CSR in vitro for 2 d, after which germline transcripts of the Sμ, Sγ1, and Sγ3 regions and messenger RNA transcripts of the β-actin locus were amplified by RT-PCR. (C) Microhomologies at the junction between the Sμ and Sγ3 regions in IgG3$^+$ *Polζ$^{f/Δ}$/CD21-cre* B cells. B cells were stimulated with LPS to undergo CSR to IgG3$^+$ for 3 d. After isolation of the DNA, the switch junctions were amplified by a nested PCR using primers that anneal in Sμ and Sγ3, subcloned, and sequenced. Black bars, *Polζ$^{+/Δ}$/CD21-cre* cells (64 sequences); gray bars, *Polζ$^{f/Δ}$/CD21-cre* cells (41 sequences). Statistical significance for changes in the frequency of sequences with insertions, no or short microhomologies (0–2 nt), and longer microhomologies (3–7 nt) in *Polζ$^{f/Δ}$/CD21-cre* cells, P = 0.04.

Polζ$^{f/Δ}$ and *Polζ$^{Δ/Δ}$* GC B cells. In *Polζ$^{Δ/Δ}$* cells, 62% of all mutations accumulated at A-T basepairs, which compared with 61% for *Polζ$^{f/Δ}$* cells (Fig. 3, B and C). Likewise, the ratio of transitions to transversions was not altered. We conclude from these data that Polζ deficiency has no impact on the pattern of SHM and that the differences in the A-T mutations observed in the bulk analysis must have been a result of differences in the fidelity of gene amplification between the experimental groups, a possibility which is excluded in the single cell analysis. With respect to the frequency of SHM, two interpretations offer themselves to explain the results: Polζ deficiency either directly impacts the SHM mechanism or it results in a rapid arrest of cellular proliferation preventing further SHM. The absence of a change of mutation pattern favors the latter interpretation.

Impaired CSR in *Polζ$^{f/Δ}$/CD21-cre* mice

To study a possible effect of Polζ deficiency on CSR, splenic B cells from *Polζ$^{f/Δ}$/CD21-cre* and control mice were stimulated with LPS in the presence or absence of IL-4, and the percentages of class-switched cells were measured by flow cytometry 3 or 4 d later. Compared with wild-type B cells, B cells from the mutant mice exhibited 2–3-fold reduced frequencies of cells switched to the expression of IgG1 or IgG3, respectively (Fig. 4 A and Table I). As CSR and cell proliferation are linked (47), we labeled *Polζ$^{f/Δ}$/CD21-cre* B cells and control cells with CFSE and measured their ability to divide. Proliferation of *Polζ$^{f/Δ}$/CD21-cre* B cells was reduced compared with controls (Fig. 4 A). Moreover, cell viability of *Polζ$^{f/Δ}$/CD21-cre* B cells dropped significantly 3 d after activation (unpublished data). Defective proliferation and decreased viability could explain the reduced frequency of Polζ-deficient cells switched to the expression of IgG1 and IgG3. However, the defect in CSR did not appear to be linked to the reduced ability of *Polζ$^{f/Δ}$/CD21-cre* B cells to

Table I. General and IgH locus-specific genomic instability in stimulated *Polζ$^{f/\Delta}$/CD21-cre* B cells measured by FISH

Genotype	Cytokine stimulation	Percentage of IgG1$^+$ cells on day 4	General genome instability			IgH locus-specific instability	
			Number of metaphases analyzed	Number of chromosomal aberrations	Number of metaphases with chromosomal breaks (%)	Number of metaphases analyzed	Number of metaphases with breaks in the IgH locus (%)
Polζ$^{f/+}$	α-CD40 + IL-4	30.3	30	1	1 (3)	50	1 (2)
CD21-cre	α-CD40 + IL-4	36.1	30	2	2 (7)	50	2 (4)
Polζ$^{f/+}$/CD21-cre	α-CD40 + IL-4	28.4	30	8	7 (23)	50	1 (2)
Polζ$^{f/+}$/CD21-cre	α-CD40 + IL-4	26.1	30	9	8 (27)	50	1 (2)
Polζ$^{f/+}$/CD21-cre	α-CD40 + IL-4	32.6	30	5	5 (17)	50	1 (2)
Polζ$^{f/+}$/CD21-cre	α-CD40 + IL-4	34.7	30	2	2 (7)	50	1 (2)
Polζ$^{f/+}$/CD21-cre	α-CD40 + IL-4	23.7	30	3	2 (7)	50	0 (0)
Polζ$^{f/+}$/CD21-cre	α-CD40	1.0	ND	ND	ND	50	0 (0)
Polζ$^{f/+}$/CD21-cre	α-CD40	0.1	28	1	1 (3)	50	0 (0)
Polζ$^{f/+}$/CD21-cre	α-RP105	0.2	22	0	0 (0)	50	0 (0)
Polζ$^{f/\Delta}$/CD21-cre	α-CD40 + IL-4	16.7	30	47	24 (80)	50	5 (10)
Polζ$^{f/\Delta}$/CD21-cre	α-CD40 + IL-4	13.0	30	41	20 (67)	50	5 (10)
Polζ$^{f/\Delta}$/CD21-cre	α-CD40 + IL-4	19.5	30	30	16 (53)	50	3 (6)
Polζ$^{f/\Delta}$/CD21-cre	α-CD40 + IL-4	16.6	30	35	14 (47)	50	3 (6)
Polζ$^{f/\Delta}$/CD21-cre	α-CD40 + IL-4	16.8	30	16	10 (33)	50	4 (8)
Polζ$^{f/\Delta}$/CD21-cre	α-CD40 + IL-4	18.0	30	19	11 (37)	50	5 (10)
Polζ$^{f/\Delta}$/CD21-cre	α-CD40	0.5	30	18	13 (43)	50	0 (0)
Polζ$^{f/\Delta}$/CD21-cre	α-CD40	0.1	20	10	7 (35)	50	0 (0)
Polζ$^{f/\Delta}$/CD21-cre	α-CD40	0.1	23	1	1 (4)	50	0 (0)
Polζ$^{f/\Delta}$/CD21-cre	α-RP105	0.1	30	29	20 (67)	50	0 (0)
Polζ$^{f/\Delta}$/CD21-cre	α-RP105	0.1	30	31	15 (50)	50	0 (0)

Each row represents the results from one individual mouse.

proliferate. The percentages of class-switched cells were also 2–3-fold reduced when cells having undergone a similar number of divisions were analyzed for CSR (Fig. 4 A, gate indicated by red bracket). The latter result was independent of the location or width of the gate.

Germline transcription of the S regions is required for the initiation of CSR. Hence, we asked whether differences of germline transcription could account for the impairment of CSR in *Polζ$^{f/\Delta}$/CD21-cre* B cells. We stimulated splenic B cells with either LPS + IL-4 or LPS alone for 2 d and then amplified germline transcripts of Sμ, Sγ1, and Sγ3 by RT-PCR. *Polζ$^{f/\Delta}$/CD21-cre* and control B cells produced similar levels of Sμ, Sγ1, and Sγ3 transcripts (Fig. 4 B). To test whether Polζ is required for the repair phase of CSR, we amplified and sequenced Sμ-Sγ3 junctions from mutant and control cells, as it is known that the inactivation of some genes involved in DNA repair, such as MSH2, PMS2, or Polη, can lead to changes in the nature of the microhomologies or mutations at the junctions between the Sμ and Sγ3 or other S regions in class-switched cells (15, 19, 48, 49). PCR products between 500 and 800 nt were selected for analysis, subcloned, and sequenced, excluding clonally related cells. We then analyzed the sequences by BLAST alignment to the germline Sμ and Sγ3 sequences and counted the number of nucleotides at the S junctions that were identical to both the Sμ and Sγ3 region. The majority (53%) of the sequences derived from *Polζ$^{+/\Delta}$/CD21-cre* B cells displayed little (1–2 nt) or no microhomology at the S junctions, whereas a smaller fraction (21%) of sequences exhibited a longer stretch (3–7 nt) of nucleotide overlap (Fig. 4 C). The remaining fraction (25%) had insertions of 1 nt or more at the S junctions. Similar to the control cells, the majority of sequences (56%) derived from *Polζ$^{f/\Delta}$/CD21-cre* B cells contained no or only small microhomologies. In contrast, the frequency of sequences containing microhomologies of 3–7 nt was increased (34%), whereas the frequency of sequences containing insertions was reduced (10%). Insertions of 2 nt or longer were absent in sequences from the mutant B cells in contrast with control sequences. The changes in the nature of the Sμ–Sγ3 junctions, albeit modest, are consistent with a possible requirement for Polζ in the efficient processing of free DNA ends during CSR.

We also analyzed the switch junctions for somatic point mutations, which are known to occur in these regions through the recruitment of AID in the initiation of CSR (13, 50). In cells initiating but not completing CSR in the course of

proliferation, such mutations are introduced into Sμ but are rarely found in Sγ1 or Sγ3. It is believed that this explains the higher load of mutations in the Sμ parts of Sμ–Sγ1 or –Sγ3 switch junctions (24, 49, 50). Comparing the sequences of Sμ–Sγ3 junctions within a 200-bp window, we found that in wild-type cells the mutation frequencies in the Sμ portions of the junctions were indeed higher than in Sγ3 portions (0.53 and 0.27%, respectively), whereas in the mutants they were similarly low (0.21 and 0.22%, respectively; Table S1, available at http://www.jem.org/cgi/content/full/jem.20080669/DC1). The limited number of mutations did not allow a meaningful comparison of the mutation pattern. These results indicate that somatic mutations were equally introduced in mutant and control cells into switch regions undergoing switch recombination but that because of impaired proliferation and survival, the mutant cells had less opportunity to accumulate mutations in Sμ before switching.

Chromosomal aberrations in *Polζ*$^{f/\Delta}$*/CD21-cre* B cells

Polζ had been previously shown to be required for genome stability in the DT40 chicken B cell line and mouse embryonic fibroblasts (51, 52). As genomic instability might explain the defective proliferation and CSR in LPS-activated Polζ-deficient B cells, as well as the counterselection of Polζ-deficient GC B cells, we stimulated B cells from two *Polζ*$^{f/\Delta}$*/CD21-cre* and two control (*Polζ*$^{f/+}$*/CD21-cre*) mice with LPS + IL-4 or LPS alone in vitro, prepared metaphase spreads 3 d later, stained the chromosomes with DAPI, and analyzed the metaphases by microscopy (Fig. 5 A). Chromosomal abnormalities were observed in 3% of the metaphases

A

genotype	metaphases analyzed	metaphases with chromosome abnormalities		chromosome abnormalities per metaphase	broken chromosomes or chromatids	chromosome fusions
Polζ$^{f/+}$/CD21-cre	39	1	(3%)	1.0	0	1
Polζ$^{f/\Delta}$/CD21-cre	33	13	(39%)	1.6	12	9

Examples of chromosome abnormalities:

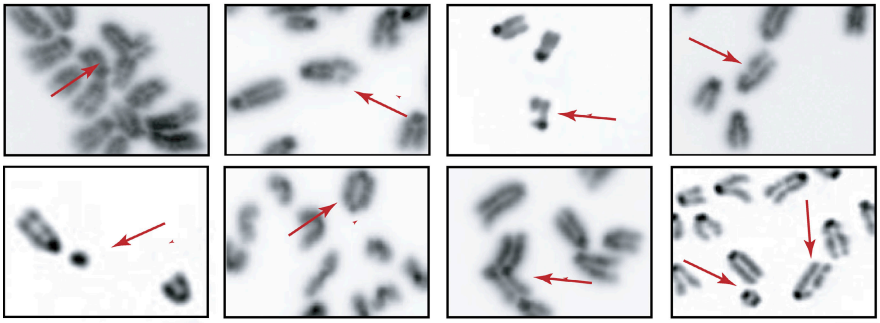

B

	metaphases analyzed	metaphases with chromosome abnormalities		broken chromosomes		chromosome translocations and fusions	
Polζ$^{f/+}$/CD21-cre	43	2	(5%)	2	chr. 7; 13	1	chr. (5; 13)
Polζ$^{f/\Delta}$/CD21-cre	42	9	(23%)	7	chr. 1; 12; 11; 11; 12; 1; 7	6	chr. (1; 3) (3; 3) (X; 15) (3; 1) (14; 1) (17; 8)

Examples of chromosome abnormalities:

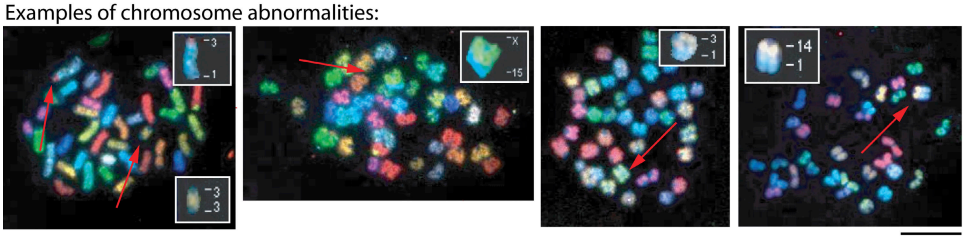

dicentric (1; 3) (3; 3) dicentric (1; 3) (3; 3) | translocation (X;15) translocation (X;15) | translocation (1; 3) translocation (1; 3) | translocation (14; 1) translocation (14

Figure 5. Chromosome stability in *Polζ*-deficient B cells. (A) Chromosome aberrations in B cells of *Polζ*$^{f/\Delta}$*/CD21-cre* mice. B cells of *Polζ*$^{f/\Delta}$*/CD21-cre* mice and control mice were activated to proliferate by the stimulation with LPS + IL-4 or LPS alone for 3 d. After induction of chromosome condensation and fixation of the cells, metaphase spreads were prepared and stained with DAPI for the visualization by fluorescence microscopy. Shown are the combined data of two mice per genotype. Bar, ∼1 μm. (B) SKY of B cell s of *Polζ*$^{f/\Delta}$*/CD21-cre* mice. After stimulation of B cells with LPS + IL-4, metaphases were prepared, hybridized with suitable probes, and examined by fluorescence microscopy. Shown are the combined data of two mice per genotype. Red arrows indicate chromosome abnormalities. Bar, ∼5 μm.

from B cells of the control mice in contrast with 39% of the metaphases from B cells of *Polζ*$^{f/\Delta}$*/CD21-cre* mice. We saw approximately equal frequencies of broken chromosomes and chromatids versus fused chromosomes in the affected metaphases of Polζ-deficient B cells. The occurrence of broken chromosomes and broken chromatids (which are present in mitotic cells as a result of unrepaired DSBs introduced before or after replication, respectively) suggested a DNA repair defect throughout the cell cycle (Fig. 5 A, Table S2 [available at http://www.jem.org/cgi/content/full/jem.20080669/DC1], and see Fig. 7). Spectral karyotyping (SKY) confirmed the general chromosomal instability detected in Polζ-deficient B cells (Fig. 5 B). Consistent with the previous analysis, only a modest number (5%) of metaphases of B cells from control mice contained irregular chromosomes, whereas metaphases containing broken chromosomes, chromosome fusions, and translocations were much more frequent (23%) in B cells of *Polζ*$^{f/\Delta}$*/CD21-cre* mice stimulated in vitro with LPS + IL-4 for 3 d. Even though Polζ-deficient metaphases were present with a broken chromosome 12, which carries the IgH locus in the mouse and where CSR occurs, other chromosomes (namely chromosomes 1, 3, and 11) were affected at a similar frequency. However, the sensitivity of either DAPI staining or SKY in the detection of CSR-specific breaks is limited, as the IgH locus is located in the subtelomeric region of chromosome 12, and such techniques may fail to distinguish an intact chromosome 12 from one lacking a small telomeric fragment as a result of a break within the IgH locus. We therefore proceeded to analyze CSR-specific chromosome breaks by fluorescence in situ hybridization (FISH) using IgH locus-specific probes.

Increase of IgH locus-specific breaks in B cells of *Polζ*$^{f/\Delta}$*/CD21-cre* mice undergoing CSR

In these experiments, we induced CSR in B cells of *Polζ*$^{f/\Delta}$*/CD21-cre* mice and of control mice by stimulation with an α-CD40 antibody in the presence of IL-4. This treatment efficiently induces CSR to IgG1 and allows comparison to stimulation with α-CD40 mAb alone, which activates the cells by itself and, in contrast with LPS, does not induce CSR. On day 4 after stimulation, metaphases were analyzed by FISH. Using a telomere-specific probe, we confirmed the increased general genome instability in B cells of *Polζ*$^{f/\Delta}$*/CD21-cre* mice in that we observed chromosomal breaks in

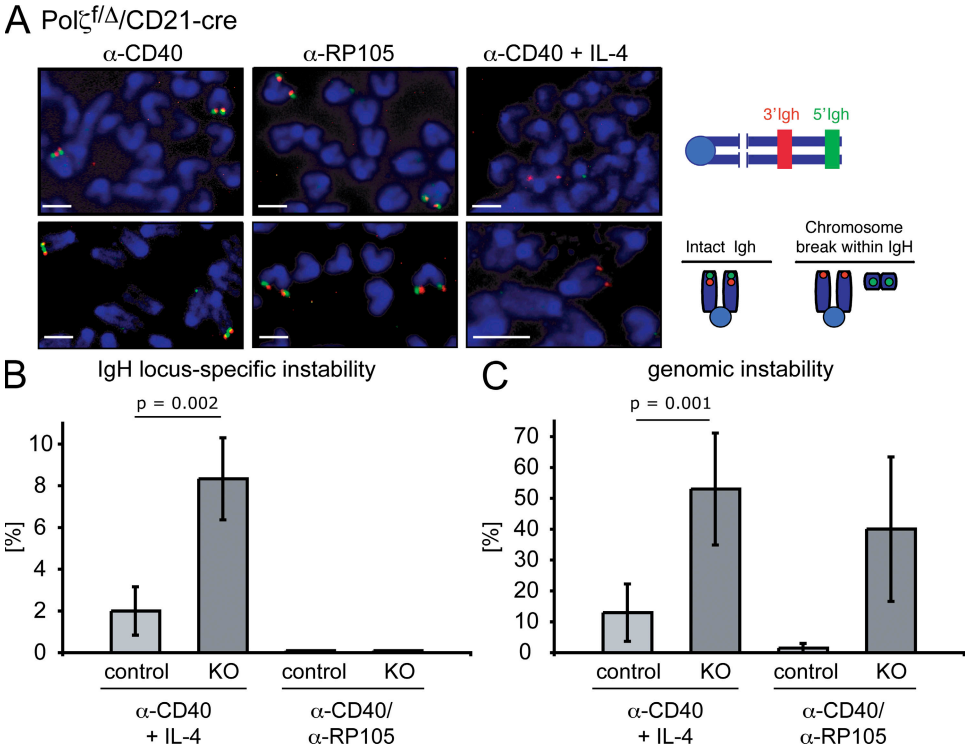

Figure 6. Genomic instability in stimulated *Polζ*$^{f/\Delta}$*/CD21-cre* B cells measured by FISH. Purified B cells were stimulated with α-CD40, α-RP105, or α-CD40 + IL-4 for 4 d. Subsequently, metaphase spreads were hybridized with either a telomere probe to measure chromosomal aberrations or with BAC probes flanking the IgH locus to measure IgH locus-specific chromosomal breaks. (A) Examples of metaphases from *Polζ*$^{f/\Delta}$*/CD21-cre* B cells hybridized with IgH locus-specific probes. Note the disappearance of the green signal of the 5′ IgH probe in cells stimulated with α-CD40 + IL-4. Bars, ∼1 µm. (B) Mean percentage of metaphases with IgH locus-specific breaks from *Polζ*$^{f/\Delta}$*/CD21-cre* and control B cells stimulated with α-CD40 + IL-4, α-CD40, or α-RP105. Results from the latter two stimuli were combined. See also Table I. (C) Mean percentage of metaphases with general chromosomal breaks from *Polζ*$^{f/\Delta}$*/CD21-cre* and control B cells stimulated with α-CD40 + IL-4, α-CD40, or α-RP105. Results from the latter two stimuli were combined. Error bars represent SD. See also Table I.

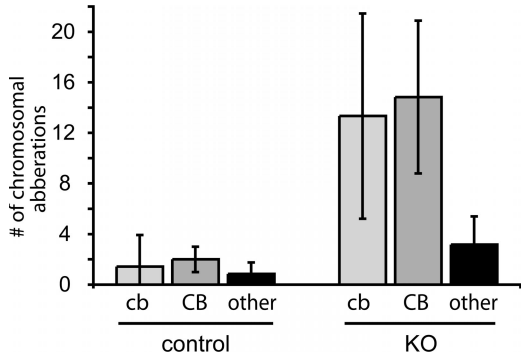

Figure 7. Types of genomic instabilities in stimulated *Polζ$^{f/\Delta}$/CD21-cre* B cells measured by telomere-specific FISH. Purified B cells were stimulated with α-CD40 + IL-4 for 4 d. Subsequently, metaphase spreads were hybridized with a telomere probe to measure chromosomal aberrations. Shown is the mean number of chromosomal aberrations per 30 metaphases from *Polζ$^{f/\Delta}$/CD21-cre* and control B cells plus the SD. cb, chromatid break; CB, chromosome break; other includes chromosomal rearrangements such as dicentric and robertsonian chromosomes. See also Table S2 (available at http://www.jem.org/cgi/content/full/jem.20080669/DC1).

53 versus 13% of all metaphases of B cells from *Polζ$^{f/\Delta}$/CD21-cre* and control (*Polζ$^{f/+}$/CD21-cre*) mice, respectively (Fig. 6 and Table I). The chromosomal breaks in B cells from both *Polζ$^{f/\Delta}$/CD21-cre* and control (*Polζ$^{f/+}$/CD21-cre*) mice consisted of approximately equal proportions of chromatid and chromosome breaks (Fig. 7 and Table S2). The results in Table S2 also raise the possibility that *Polζ* haploinsufficiency affects genome stability in cells activated to undergo CSR, but more data would be required to firmly establish this point.

To assay for breaks or translocations within the IgH locus, we used a FISH assay in which the first probe recognizes sequences just upstream of the IgH V_H domain on the telomeric region of chromosome 12 (5′ Igh probe) and the second probe sequences immediately downstream of the C_H locus (3′ Igh probe) (26). This assay revealed chromosomal breaks within the IgH locus, visualized as separated 3′ and 5′ IgH signals, in 8.3% of metaphases from α-CD40 mAb + IL-4–activated B cells from *Polζ$^{f/\Delta}$/CD21-cre* mice. This is in contrast with only 2% of metaphases containing such breaks in activated control B cells (Fig. 6 and Table I). The breaks led to IgH locus-specific translocations in 28% of the affected cells from *Polζ$^{f/\Delta}$/CD21-cre* mice and in 43% of affected control B cells (unpublished data). These findings suggest that Polζ is required for repair of a subset of IgH locus breaks that occur during CSR.

To ensure that the enhancement of IgH breaks in activated *Polζ$^{f/\Delta}$/CD21-cre* B cells is indeed caused by CSR, we also stimulated B cells from *Polζ$^{f/\Delta}$/CD21-cre* and control mice with an α-CD40 or α-RP105 mAb alone because such treatments induce proliferation but not CSR (53). Although B cells of *Polζ$^{f/\Delta}$/CD21-cre* mice again accumulated chromosomal aberrations at a higher level than the control cells, IgH locus-specific breaks were not detected in either cell type under these conditions (Fig. 6, B and C; and Table I). We conclude that the increased frequency of chromosomal breaks in the IgH loci in B cells from *Polζ$^{f/\Delta}$/CD21-cre* mice after α-CD40 mAb + IL-4 stimulation is a result of defective repair of CSR-induced DSBs.

DISCUSSION

Ubiquitous Polζ deficiency in the mouse is embryonic lethal (39–41). We have overcome this lethality by generating a conditional allele of *Rev3* and used this allele to render mature resting CD21-expressing B cells deficient of Polζ. Using this system, we show that Polζ is not essential for B cell maintenance but is required for proper B cell proliferation, presumably because of its role in the maintenance of genome stability. The genomic instability and proliferation defect of Polζ-deficient B cells observed in the present study is reminiscent of the phenotype of Polζ-deficient chicken DT40 B cells, which also accumulate genomic aberrations and are impaired in their ability to proliferate (52). Genomic instability was also observed in Polζ-deficient mouse embryonic fibroblasts, which barely divide and require inactivation of p53 to proliferate (51). It has been speculated that Polζ may prevent the collapse of replication forks that have stalled at DNA lesions and may facilitate postreplication DNA repair via homologous recombination or translesion synthesis and mismatch extension (42, 51). However, the role of Polζ in the maintenance of genome stability has not been determined with precision. Many components of the NHEJ or DNA damage response machinery do not affect proliferation and SHM (24, 28, 54). B cells deficient of the classical NHEJ factors Xrcc4 and ligase 4 harbor predominantly chromosome breaks, which are indicative of failed DSB repair in the G1 phase of the cell cycle (23). In contrast, we found high frequencies of both chromosome and chromatid breaks in the Polζ-deficient B cells, indicating pre- and postreplication repair defects, respectively. It is thus also conceivable that the impaired proliferation and reduced cell viability of Polζ-deficient B cells are a result of a function of Polζ in NHEJ, translesion synthesis, and homologous recombination.

Genomic instability and impaired proliferative capacity of Polζ-deficient B cells are likely the main reasons for the impaired GC and IgG1 antibody response in our mutant animals, in which Polζ was selectively ablated in mature B cells. GCs were reduced in size, the frequency of somatic mutations introduced into V region genes was reduced, and CSR was impaired. We also observed counterselection of cells that had undergone deletion of the *Rev3* gene in GCs. Analyzing the extent and pattern of SHM in Polζ-proficient and -deficient GC B cells by single cell PCR, we found a >3.5-fold reduction of the frequency of somatic mutations in the mutant cells but no change in the mutational pattern. Given that Polη has been identified as the sole polymerase responsible for mutations at A-T basepairs (55), a contribution of Polζ to SHM should have resulted in a change of the mutational pattern in Polζ-deficient B cells. In the absence of such a change, our results are consistent with the interpretation that the

impairment of SHM by Polζ deficiency is caused by the impaired cell viability and consequent counterselection of the mutant cells in the GC reaction.

In two earlier papers a direct involvement of Polζ in the mechanism of SHM had been suggested (37, 38). In one approach, Diaz et al. (37) constitutively expressed antisense RNA against Polζ in transgenic mice and observed compromised SHM in the absence of a change of mutational pattern, which is similar to the present data. Although these results were difficult to interpret because of the non–B cell-autonomous expression of the transgenic antisense RNA and possible genomic instability also in that system, a study of SHM in a Burkitt lymphoma cell line again demonstrated a reduced frequency of somatic mutation upon transfection of the cells with Rev3-specific antisense oligonucleotides, without an effect on the mutation pattern (37, 38). Rev3 expression was only partially inhibited in these experiments, and cell proliferation was not detectably affected. It remains to be seen to which extent these latter experiments reflect the requirements for SHM in GC B cells in vivo, where a direct participation of Polζ in its control clearly remains tentative.

In contrast with SHM, where our results suggest indirect effects of Polζ deficiency, our data indicate a direct involvement of Polζ in CSR. We observed a reduction in CSR efficiency of Polζ-deficient B cells compared with control B cells even when we compared cells that had gone through the same number of cell divisions. Together with the observation that germline transcription of the S regions remains unaffected in *Polζ*$^{f/\Delta}$*/CD21-cre* mice, this suggested an involvement of Polζ in the repair phase of CSR, a notion which was directly supported by the increased frequency of IgH locus-specific DNA breaks in Polζ-deficient B cells undergoing CSR in response to anti-CD40 stimulation in the presence of IL-4. Our evidence clearly indicates that these breaks were caused by a defective CSR process because they were absent in Polζ-deficient B cells activated with α-CD40 or α-RP105 mAbs alone, an activation protocol which induces proliferation but not CSR. Among 1,200 chromosomes analyzed by telomere FISH from individual α-CD40 + IL-4 cultures, ∼3% of the chromosomes from Polζ-deficient B cells showed abnormalities including chromatid breaks, chromosome breaks, and chromosome fusions (Fig. 7, Table I, and Table S2). However, telomere FISH does not distinguish between CSR-specific and -unspecific chromosomal aberrations. To approach this problem, we determined the frequency of such CSR-specific breaks in the activated Polζ-deficient cells within the IgH locus on chromosome 12, where CSR occurs. Based on the genome instability detected by telomere FISH, we estimated that if chromosome 12 was targeted randomly, three breaks in this chromosome should be found among 50 metaphases and these breaks should be randomly distributed along the chromosome. In contrast with the latter prediction, we detected three to five IgH locus-specific chromosome breaks in 50 metaphases (Table I). Considering that the IgH locus covers only ∼3% of chromosome 12, this implies that IgH locus-specific breaks in Polζ-deficient B cells stimulated to undergo CSR are the result of a targeted rather than a random process. In further support of this notion, we failed to observe chromatid breaks at the IgH locus in metaphases of Polζ-deficient cells (in contrast with their frequent occurrence at other loci), suggesting that, specifically within the IgH locus, Polζ functions to repair a subset of DSBs restricted to prereplicative stages of the cell cycle (G1) precisely when AID is known to target S regions (13, 56). In principle, an increased frequency of IgH locus-specific DNA breaks could also result from defective V(D)J recombination. This has been recently observed in ATM-deficient B cells, which accumulate such breaks in an AID-independent and RAG-dependent manner (53). Because the *CD21-cre* allele causes the deletion of the floxed *Polζ* allele in mature but not developing B cells (44) and no IgH locus-specific DNA breaks were detected in Polζ-deficient B cells stimulated with α-CD40 or α-RP105 mAbs, such a possibility seems to be excluded in the present context.

CSR involves the generation of staggered DSBs during the G1 phase of the cell cycle, which need to be processed to create blunt DNA ends that serve as substrates for the alternative and classical NHEJ machinery (13, 23, 56–58). This processing requires the activity of exonucleases and DNA polymerases, with the former being provided by exonuclease 1 among perhaps other enzymes (20). The present results suggest that Polζ catalyzes fill-in reactions in the course of CSR-associated DSB repair by NHEJ. This is in line with observations in *Saccharomyces cerevisiae* that ATR homologue Mec1-dependent phosphorylation, which plays a major role in DNA damage checkpoint responses, promotes the association of Polζ/Rev1 with DSBs (59, 60). Our observation that CSR is impaired in the absence of Polζ, yet not completely abolished, points to the participation of additional polymerases in the repair phase of CSR. These could include Polμ and Polλ, both of which have been suggested to operate in classical NHEJ (61, 62).

In normal B cells undergoing CSR, strict dosing of AID and efficient repair by NHEJ prevents aberrant rejoining of IgH locus-specific DSBs to DSBs within other loci. Dysregulation of AID activity or deficiency of specific repair factors has been shown to increase the frequency of oncogenic IgH-myc translocations in in vitro cultured primary B cells undergoing CSR (27). In this context, we report frequent chromosomal translocations involving the IgH locus (and multiple uncharacterized partners) in primary Polζ-deficient B cells undergoing CSR in vitro. We also observed a slight trend toward increased genomic instability in *Polζ*$^{f/+}$*/CD21-cre* heterozygous B cells compared with wild-type B cells (Table S2). Thus, genetic or epigenetic alterations that result in Polζ (haplo) insufficiency might act in vivo to increase the frequency of oncogenic IgH locus translocations.

MATERIALS AND METHODS

Targeting vector and generation of gene-targeted mice. A 25-kb clone comprising 4 exons of rev3 was obtained by screening a P1 library generated from C57BL/6 genomic DNA. The clone was used to construct

a targeting vector containing a loxP-flanked exon 2. The culture and transfection of C57BL/6-derived Bruce4 ES cells has been described previously. Homologous recombination was determined by Southern hybridization of probe A with EcoRI-digested genomic DNA or of probe B with BamHI-digested genomic DNA. The latter assay was also used to ensure the integration of the third loxP site. After homologous recombination, the *neomycin resistance* gene was removed in vitro by transfection of ES cells with the Cre recombinase-expressing plasmid pIC-Cre. Two independently targeted ES cell clones were injected into CB.20-derived blastocysts, which were implanted into pseudo-pregnant CB.20 foster mice to generate chimeric mice. Both clones transmitted the targeted allele into the germline. The correct targeting was confirmed by a nested PCR. The first PCR round used the primers polz-1 [5′-GTCCGTCTGCCATCAAGTCTAGCTTCAG-3′] and polz-2 [5′-GGAAGCCCTGGATTTCATCACGCCATTG-3′], which anneal 5′ of the region of homology and 3′ of the second loxP site, respectively (Fig. 1 B). Both the $Pol\zeta^{+}$ and $Pol\zeta^{f}$ allele yielded a PCR product of ~5.2 kb. This was followed by an amplification step of the gel-purified PCR products using primers that flank each loxP site (first loxP site: primers polz-3 [5′-GTCAGCTGGTCAGAGTGAGGGATAC-3′] and polz-4 [5′-TAACCAGCACACTACCACTACCTGGG-3′]; second *loxP* site: primers polz-5 [5′-CCTCCTCAGTAGTAGTAGGACCTTTGGAGG-3′] and polz-6 [5′-CGTATCTGCCCACTCTCTGTCATTCTCTC-3′]). The primers polz-1 and polz-2 were also used for the amplification of the $Pol\zeta^{\Delta}$ allele from tail DNA of $Pol\zeta^{+/\Delta}$ mice. Parts of the PCR product (3.2 kb) were sequenced using the primers polz-1, polz-3, and polz-6 to confirm the integration of the targeting vector into the *Rev3* locus and the excision of exon 2.

Mice. $Pol\zeta^{f/+}$ mice were intercrossed with *deleter* mice to obtain mice carrying a nonfunctional *Polζ* allele ($Pol\zeta^{\Delta/+}$ mice) (45). Subsequent intercrosses between $Pol\zeta^{f/+}$ mice, $Pol\zeta^{\Delta/+}$ mice, and *CD21-cre* mice generated $Pol\zeta^{f/\Delta}$/*CD21-cre* mice (44). The mice were kept on a C57BL/6 background. All mouse experiments were approved by the Institutional Animal Care and Use Committee of Harvard University and by the Immune Disease Institute.

Flow cytometry. Single-cell suspensions prepared from lymphoid organs were stained with the following monoclonal antibodies conjugated to FITC, PE, CyC, APC, or biotin: anti-CD3 (145-2C11), anti-CD4 (L3T4), anti-CD8 (53–6.7), anti-CD19 (ID3), anti-CD21, anti-CD23 (B3B4), anti-CD43 (S7), and anti-Fas (Jo2; BD). Monoclonal antibodies against IgM (R33-2412) and B220 (RA3-6B2) were prepared and conjugated in our laboratory. PNA conjugates were PNA-FITC or PNA-biotin (Vector Laboratories). Biotin conjugates were visualized with CyC or APC-streptavidin (BD). All samples were acquired on a FACSCalibur (BD) and analyzed using CellQuest software (BD).

Immunizations. Mice were immunized by intraperitoneal injection with 100 μg of alum-precipitated NP_{36}-CG ((4-hydroxy-3-nitrophenyl)acetyl coupled to chicken γ-globulin; Biosearch Technologies, Inc.). NP-specific Ig serum titers were monitored every 7 d by bleeding of the mice from the tail vein and subsequent ELISA.

Deletion efficiency of the $Pol\zeta^{f}$ allele in GC B cells. $CD19^{+}PNA^{low}Fas^{low}$ naive and $CD19^{+}PNA^{high}Fas^{high}$ GC B cells were sorted by FACS, subsequently lysed in 50 μl of 10-mM Tris, ph 7.5, plus 250 μg/ml proteinase K for 3 h at 56°C, and heat inactivated for 15 min at 80°C. Serial dilutions of 20,000 cell equivalents were used for the amplification of the $Pol\zeta^{f}$ and $Pol\zeta^{\Delta}$ alleles in a competitive PCR (30 s and 94°C denaturation; 30 s and 67°C annealing; and 1 min and 72°C elongation, 30 cycles) using the forward primers Seq1 (5′-AAAGGTCAGCTGGTCAGAGTGAGGGA-3′) and Seq7 (5′-ATGTAAAAGAATACAGTGGAAGTGAGG-3′), which anneal 5′ and within the floxed region, respectively, and the common reverse primer Seq2, 5′-GGGAAGCCCTGGATTTCATCACG-3′, which anneals 3′ of the floxed region. The ratios of the $Pol\zeta^{f}$- and $Pol\zeta^{\Delta}$-derived PCR fragments were compared with a standard curve of known ratios to estimate the deletion efficiency.

Analysis of SHM. Single GC B cells ($CD19^{+}PNA^{high}Fas^{high}$) were sorted by flow cytometry into 96-well plates and analyzed individually using a nested PCR for the genotyping of the cells and a seminested PCR for the amplification of DNA fragments corresponding to the introns downstream of the rearranged $V_HD_HJ_H$ elements. After cell lysis with proteinase K in PCR buffer, the PCR was performed amplifying DNA fragments corresponding to the $Pol\zeta^{f}$ and $Pol\zeta^{\Delta}$ using the primers zeta1 (5′-ACCAAAAGAAAGGTCAGCTGGTCAGAGTGAGGG-3′), zeta3 (5′-TTTTAGACTGGGTGCTCAGGAAGGGTCTCATTGAC-3′), and zeta6 (5′-TGCTCTTGTACTCAGAGACTGGCTCACGGAGC-3′) and DNA fragments containing the introns downstream of the rearranged $V_HD_HJ_H$ elements using the primers J558Fr3 (5′-CAGCCTGACATCTGAGGACTCTGC-3′) and JH4-int2 (5′-GCTCCACCAGACCTCTCTAGACAGC-3′), which anneal in the framework 3 region of most V_HJ558 elements and the intron downstream of J_H4, respectively (46). The annealing temperature was five cycles at 62°C followed by five cycles at 60°C and 30 cycles at 58°C. The second PCR reactions for the amplification of the *Polζ* alleles and the IgH introns were performed separately using 5 μl of the initial PCR reaction mix. The deletion of the $Pol\zeta^{f}$ allele was determined with the primers zeta4 (5′-AAGAATACAGTGGAAGTGAGGGAGCAGGATCCG-3′) and zeta5 (5′-CCTATGGGAAGCCCTGGATTTCATCACGC-3′) detecting the $Pol\zeta^{f}$ allele and the primers zeta5 and zeta2 (5′-TGCAAGGTACTGACGAGCAACATGAGAAATATGGG-3′) detecting the $Pol\zeta^{\Delta}$ allele. The IgH introns were amplified with the primers J558Fr3 and JH4Hint-1 (5′-TGCCTTTCTCCCTTGACTCAATCAC-3′). The annealing temperature of the secondary PCR reactions was 58°C. DNA products corresponding to the JH introns were directly sequenced with the primers J558Fr3 and JH-4Hint-1. To compare the frequency of somatic mutations, a 500-bp stretch downstream of the rearranged J_H gene segments was analyzed for the accumulation of somatic mutations. Cells carrying only deleted Polζ alleles ($Pol\zeta^{\Delta/\Delta}$) were grouped and compared with cells from the same mouse that retained a floxed Polζ allele ($Pol\zeta^{f/\Delta}$). To compare the pattern of somatic mutations, the mutations were analyzed in each J_H intron and subsequently normalized according to the base composition of the individual J_H intronic regions analyzed (intronic region J_H1 [A, 0.97; C, 1.147; G, 1.04; T, 0.87], intronic region J_H2 [A, 1.15; C, 0.94; G, 1.06; T: 0.88]; intronic region J_H3 [A, 1.08; C, 1.28; G, 0.83; T, 0.91], and intronic region J_H4 [A, 0.94; C, 1.56; G, 0.92; T, 0.82]).

The analysis of SHM in GC B cells by bulk PCR has been published previously (32, 33). Splenic GC B cells were sorted into a naive fraction ($CD19^{+}PNA^{low}Fas^{low}$) and a GC fraction ($CD19^{+}PNA^{high}Fas^{high}$). PCR fragments corresponding to the intron downstream of J_H4 were obtained from DNA of purified cell populations using the primers J558Fr3 and JHCHint-1 (46). PCR fragments containing VDJ rearrangements involving a J_H4 element were selected for further analysis, subcloned, and sequenced. A stretch of 500 bp of intron sequence immediately downstream of the J_H4 element was analyzed for somatic mutations.

Class switch analysis. B cells were purified from splenic single cell suspensions by MACS depletion using anti-CD43 microbeads (Miltenyi Biotech). The cells were stimulated with either 20 μg/ml LPS alone, 20 μg/ml LPS and 25 ng/ml IL-4 (R&D Systems), or 1 μg/ml anti-CD40 mAb (clone HM40-3; BD) and 25 ng/ml IL-4. Cells were cultured for 4–5 d. The percentage of class-switched cells was determined between days 3 and 5 by flow cytometry. Proliferation was determined by labeling of the cells before stimulation with 2.5 mM CFSE in PBS and measuring the number of cell divisions on day 4 by flow cytometry. For the analysis of the switch junctions, DNA was isolated from the cells on day 3 and amplified by a nested PCR reaction using the primers Cμ1.1 and Cγ1.1, followed by Cμ1.2 and Cγ1.2. PCR products with a length of 500–800 nt were subcloned and subsequently sequenced. Clonally related sequences were excluded from the analysis.

Cytogenetic analysis. MACS-purified B cells were stimulated with 20 μg/ml LPS and 25 ng/ml IL-4 and cultured for 3 d, at which 50 ng/ml colcemid (KaryoMAX Solution; Invitrogen) was added to the medium for 2 h. The preparation of metaphases has been described elsewhere. In brief, the cells

were swelled in 0.4% potassium chloride solution for 10 min at 37°C, incubated four times in 3:1 methanol/acetic acid solution, dropped onto microscopy slides, and subsequently passed through hot steam and air dried. The metaphases were either covered with DAPI-containing mounting medium (Vectashield; Vector Laboratories) or further processed for SKY using the SkyPaint DNA kit (Applied Spectral Imaging) according to the manufacturer's instructions. The analyses were performed on a microscope (Eclipse; Nikon) using a black and white 12-bit charge-coupled device camera (Applied Spectral Imaging) and a 63× objective lens. The cytogenetic analysis by FISH has been published elsewhere (26). In brief, the cells were stimulated with 1 μg/ml of an α-CD40 mAb (clone HM1-3; BD), 2.5 μg/ml of an α-RP105 mAb (anti-CD180; clone RP/14; eBioscience), or an α-CD40 mAb and 25 ng/ml IL-4 for 4 d. Subsequently, metaphases were prepared as described and hybridized with the fluorescence-labeled BAC207 and BAC199 for the detection of the 5′ and 3′ ends of the IgH locus, respectively. The telomeres were stained with an Cy3-conjugated $(TTAGGG)_3$ PNA probe (Applied Biosystems).

Online supplemental material. Fig. S1 contains the analysis of SHM in GC B cells of *Polζ*$^{f/\Delta}$*/CD21-cre* mice and control mice by bulk PCR. Table S1 shows the frequency of mutations in Sμ and Sγ3 regions near Sμ–Sγ3 junctions in Polζ-deficient and control B cells, and Table S2 describes the types of genomic abnormalities observed in stimulated Polζ-deficient and control B cells. Online supplemental material is available at http://www.jem.org/cgi/content/full/jem.20080669/DC1.

We thank Angela Egert, Anthony Monti, Margaret Curnutte, and Victoria Dreier for expert mouse work. We also appreciate the helpful advice and comments of Sergei Koralov, Stefano Casola, Marc Schmidt-Supprian, John Manis, and Daniel Stetson.

This work was supported by the Deutsche Forschungsgemeinschaft (SFB 243) and the National Institutes of Health (grants AI054636 and CA092625 to K. Rajewsky and AI31541 and CA092625 to F.W. Alt). F.W. Alt is an Investigator of the Howard Hughes Medical Institute.

The authors have no conflicting financial interests.

Submitted: 31 March 2008
Accepted: 21 January 2009

REFERENCES

1. Rajewsky, K. 1996. Clonal selection and learning in the antibody system. *Nature*. 381:751–758.
2. McKean, D., K. Huppi, M. Bell, L. Staudt, W. Gerhard, and M. Weigert. 1984. Generation of antibody diversity in the immune response of BALB/c mice to influenza virus hemagglutinin. *Proc. Natl. Acad. Sci. USA*. 81:3180–3184.
3. Kocks, C., and K. Rajewsky. 1988. Stepwise intraclonal maturation of antibody affinity through somatic hypermutation. *Proc. Natl. Acad. Sci. USA*. 85:8206–8210.
4. Manis, J.P., M. Tian, and F.W. Alt. 2002. Mechanism and control of class-switch recombination. *Trends Immunol*. 23:31–39.
5. Muramatsu, M., K. Kinoshita, S. Fagarasan, S. Yamada, Y. Shinkai, and T. Honjo. 2000. Class switch recombination and hypermutation require activation-induced cytidine deaminase (AID), a potential RNA editing enzyme. *Cell*. 102:553–563.
6. Petersen-Mahrt, S.K., R.S. Harris, and M.S. Neuberger. 2002. AID mutates *E. coli* suggesting a DNA deamination mechanism for antibody diversification. *Nature*. 418:99–103.
7. Neuberger, M.S., R.S. Harris, J. Di Noia, and S.K. Petersen-Mahrt. 2003. Immunity through DNA deamination. *Trends Biochem. Sci*. 28:305–312.
8. Rada, C., G.T. Williams, H. Nilsen, D.E. Barnes, T. Lindahl, and M.S. Neuberger. 2002. Immunoglobulin isotype switching is inhibited and somatic hypermutation perturbed in UNG-deficient mice. *Curr. Biol*. 12:1748–1755.
9. Imai, K., G. Slupphaug, W.I. Lee, P. Revy, S. Nonoyama, N. Catalan, L. Yel, M. Forveille, B. Kavli, H.E. Krokan, et al. 2003. Human uracil-DNA glycosylase deficiency associated with profoundly impaired immunoglobulin class-switch recombination. *Nat. Immunol*. 4:1023–1028.
10. Revy, P., T. Muto, Y. Levy, F. Geissmann, A. Plebani, O. Sanal, N. Catalan, M. Forveille, R. Dufourcq-Labelouse, A. Gennery, et al. 2000. Activation-induced cytidine deaminase (AID) deficiency causes the autosomal recessive form of the Hyper-IgM syndrome (HIGM2). *Cell*. 102:565–575.
11. Schrader, C.E., E.K. Linehan, S.N. Mochegova, R.T. Woodland, and J. Stavnezer. 2005. Inducible DNA breaks in Ig S regions are dependent on AID and UNG. *J. Exp. Med*. 202:561–568.
12. Guikema, J.E., E.K. Linehan, D. Tsuchimoto, Y. Nakabeppu, P.R. Strauss, J. Stavnezer, and C.E. Schrader. 2007. APE1- and APE2-dependent DNA breaks in immunoglobulin class switch recombination. *J. Exp. Med*. 204:3017–3026.
13. Petersen, S., R. Casellas, B. Reina-San-Martin, H.T. Chen, M.J. Difilippantonio, P.C. Wilson, L. Hanitsch, A. Celeste, M. Muramatsu, D.R. Pilch, et al. 2001. AID is required to initiate Nbs1/gamma-H2AX focus formation and mutations at sites of class switching. *Nature*. 414:660–665.
14. Rada, C., J.M. Di Noia, and M.S. Neuberger. 2004. Mismatch recognition and uracil excision provide complementary paths to both Ig switching and the A/T-focused phase of somatic mutation. *Mol. Cell*. 16:163–171.
15. Schrader, C.E., J. Vardo, and J. Stavnezer. 2002. Role for mismatch repair proteins Msh2, Mlh1, and Pms2 in immunoglobulin class switching shown by sequence analysis of recombination junctions. *J. Exp. Med*. 195:367–373.
16. Chaudhuri, J., U. Basu, A. Zarrin, C. Yan, S. Franco, T. Perlot, B. Vuong, J. Wang, R.T. Phan, A. Datta, et al. 2007. Evolution of the immunoglobulin heavy chain class switch recombination mechanism. *Adv. Immunol*. 94:157–214.
17. Rooney, S., J. Chaudhuri, and F.W. Alt. 2004. The role of the non-homologous end-joining pathway in lymphocyte development. *Immunol. Rev*. 200:115–131.
18. Schrader, C.E., J. Vardo, and J. Stavnezer. 2003. Mlh1 can function in antibody class switch recombination independently of Msh2. *J. Exp. Med*. 197:1377–1383.
19. Ehrenstein, M.R., C. Rada, A.M. Jones, C. Milstein, and M.S. Neuberger. 2001. Switch junction sequences in PMS2-deficient mice reveal a microhomology-mediated mechanism of Ig class switch recombination. *Proc. Natl. Acad. Sci. USA*. 98:14553–14558.
20. Bardwell, P.D., C.J. Woo, K. Wei, Z. Li, A. Martin, S.Z. Sack, T. Parris, W. Edelmann, and M.D. Scharff. 2004. Altered somatic hypermutation and reduced class-switch recombination in exonuclease 1-mutant mice. *Nat. Immunol*. 5:224–229.
21. Kracker, S., Y. Bergmann, I. Demuth, P.O. Frappart, G. Hildebrand, R. Christine, Z.Q. Wang, K. Sperling, M. Digweed, and A. Radbruch. 2005. Nibrin functions in Ig class-switch recombination. *Proc. Natl. Acad. Sci. USA*. 102:1584–1589.
22. Reina-San-Martin, B., M.C. Nussenzweig, A. Nussenzweig, and S. Difilippantonio. 2005. Genomic instability, endoreduplication, and diminished Ig class-switch recombination in B cells lacking Nbs1. *Proc. Natl. Acad. Sci. USA*. 102:1590–1595.
23. Yan, C.T., C. Boboila, E.K. Souza, S. Franco, T.R. Hickernell, M. Murphy, S. Gumaste, M. Geyer, A.A. Zarrin, J.P. Manis, et al. 2007. IgH class switching and translocations use a robust non-classical end-joining pathway. *Nature*. 449:478–482.
24. Reina-San-Martin, B., S. Difilippantonio, L. Hanitsch, R.F. Masilamani, A. Nussenzweig, and M.C. Nussenzweig. 2003. H2AX is required for recombination between immunoglobulin switch regions but not for intra-switch region recombination or somatic hypermutation. *J. Exp. Med*. 197:1767–1778.
25. Reina-San-Martin, B., H.T. Chen, A. Nussenzweig, and M.C. Nussenzweig. 2004. ATM is required for efficient recombination between immunoglobulin switch regions. *J. Exp. Med*. 200:1103–1110.
26. Franco, S., M. Gostissa, S. Zha, D.B. Lombard, M.M. Murphy, A.A. Zarrin, C. Yan, S. Tepsuporn, J.C. Morales, M.M. Adams, et al. 2006. H2AX prevents DNA breaks from progressing to chromosome breaks and translocations. *Mol. Cell*. 21:201–214.
27. Ramiro, A.R., M. Jankovic, E. Callen, S. Difilippantonio, H.T. Chen, K.M. McBride, T.R. Eisenreich, J. Chen, R.A. Dickins, S.W. Lowe,

et al. 2006. Role of genomic instability and p53 in AID-induced c-myc-Igh translocations. *Nature*. 440:105–109.
28. Manis, J.P., J.C. Morales, Z. Xia, J.L. Kutok, F.W. Alt, and P.B. Carpenter. 2004. 53BP1 links DNA damage-response pathways to immunoglobulin heavy chain class-switch recombination. *Nat. Immunol.* 5:481–487.
29. Delbos, F., A. De Smet, A. Faili, S. Aoufouchi, J.C. Weill, and C.A. Reynaud. 2005. Contribution of DNA polymerase η to immunoglobulin gene hypermutation in the mouse. *J. Exp. Med.* 201:1191–1196.
30. Bertocci, B., A. De Smet, E. Flatter, A. Dahan, J.C. Bories, C. Landreau, J.C. Weill, and C.A. Reynaud. 2002. Cutting edge: DNA polymerases mu and lambda are dispensable for Ig gene hypermutation. *J. Immunol.* 168:3702–3706.
31. Faili, A., S. Aoufouchi, E. Flatter, Q. Gueranger, C.A. Reynaud, and J.C. Weill. 2002. Induction of somatic hypermutation in immunoglobulin genes is dependent on DNA polymerase iota. *Nature*. 419:944–947.
32. Schenten, D., V.L. Gerlach, C. Guo, S. Velasco-Miguel, C.L. Hladik, C.L. White, E.C. Friedberg, K. Rajewsky, and G. Esposito. 2002. DNA polymerase kappa deficiency does not affect somatic hypermutation in mice. *Eur. J. Immunol.* 32:3152–3160.
33. Esposito, G., G. Texido, U.A. Betz, H. Gu, W. Muller, U. Klein, and K. Rajewsky. 2000. Mice reconstituted with DNA polymerase beta-deficient fetal liver cells are able to mount a T cell-dependent immune response and mutate their Ig genes normally. *Proc. Natl. Acad. Sci. USA*. 97:1166–1171.
34. Masuda, K., R. Ouchida, A. Takeuchi, T. Saito, H. Koseki, K. Kawamura, M. Tagawa, T. Tokuhisa, T. Azuma, and J. O-Wang. 2005. DNA polymerase theta contributes to the generation of C/G mutations during somatic hypermutation of Ig genes. *Proc. Natl. Acad. Sci. USA*. 102:13986–13991.
35. Zan, H., N. Shima, Z. Xu, A. Al-Qahtani, A.J. Evinger Iii, Y. Zhong, J.C. Schimenti, and P. Casali. 2005. The translesion DNA polymerase theta plays a dominant role in immunoglobulin gene somatic hypermutation. *EMBO J.* 24:3757–3769.
36. Johnson, R.E., M.T. Washington, L. Haracska, S. Prakash, and L. Prakash. 2000. Eukaryotic polymerases iota and zeta act sequentially to bypass DNA lesions. *Nature*. 406:1015–1019.
37. Diaz, M., L.K. Verkoczy, M.F. Flajnik, and N.R. Klinman. 2001. Decreased frequency of somatic hypermutation and impaired affinity maturation but intact germinal center formation in mice expressing antisense RNA to DNA polymerase zeta. *J. Immunol.* 167:327–335.
38. Zan, H., A. Komori, Z. Li, A. Cerutti, A. Schaffer, M.F. Flajnik, M. Diaz, and P. Casali. 2001. The translesion DNA polymerase zeta plays a major role in Ig and bcl-6 somatic hypermutation. *Immunity*. 14:643–653.
39. Bemark, M., A.A. Khamlichi, S.L. Davies, and M.S. Neuberger. 2000. Disruption of mouse polymerase zeta (Rev3) leads to embryonic lethality and impairs blastocyst development in vitro. *Curr. Biol.* 10:1213–1216.
40. Esposito, G., I. Godindagger, U. Klein, M.L. Yaspo, A. Cumano, and K. Rajewsky. 2000. Disruption of the Rev3l-encoded catalytic subunit of polymerase zeta in mice results in early embryonic lethality. *Curr. Biol.* 10:1221–1224.
41. Wittschieben, J., M.K. Shivji, E. Lalani, M.A. Jacobs, F. Marini, P.J. Gearhart, I. Rosewell, G. Stamp, and R.D. Wood. 2000. Disruption of the developmentally regulated Rev3l gene causes embryonic lethality. *Curr. Biol.* 10:1217–1220.
42. Gan, G.N., J.P. Wittschieben, B.O. Wittschieben, and R.D. Wood. 2008. DNA polymerase zeta (pol zeta) in higher eukaryotes. *Cell Res.* 18:174–183.
43. Van Sloun, P.P., R.J. Romeijn, and J.C. Eeken. 1999. Molecular cloning, expression and chromosomal localisation of the mouse Rev3l gene, encoding the catalytic subunit of polymerase zeta. *Mutat. Res.* 433:109–116.
44. Kraus, M., M.B. Alimzhanov, N. Rajewsky, and K. Rajewsky. 2004. Survival of resting mature B lymphocytes depends on BCR signaling via the Igalpha/beta heterodimer. *Cell*. 117:787–800.
45. Schwenk, F., U. Baron, and K. Rajewsky. 1995. A cre-transgenic mouse strain for the ubiquitous deletion of loxP- flanked gene segments including deletion in germ cells. *Nucleic Acids Res.* 23:5080–5081.
46. Jolly, C.J., N. Klix, and M.S. Neuberger. 1997. Rapid methods for the analysis of immunoglobulin gene hypermutation: application to transgenic and gene targeted mice. *Nucleic Acids Res.* 25:1913–1919.
47. Rush, J.S., M. Liu, V.H. Odegard, S. Unniraman, and D.G. Schatz. 2005. Expression of activation-induced cytidine deaminase is regulated by cell division, providing a mechanistic basis for division-linked class switch recombination. *Proc. Natl. Acad. Sci. USA*. 102:13242–13247.
48. Zeng, X., G.A. Negrete, C. Kasmer, W.W. Yang, and P.J. Gearhart. 2004. Absence of DNA polymerase η reveals targeting of C mutations on the nontranscribed strand in immunoglobulin switch regions. *J. Exp. Med.* 199:917–924.
49. Faili, A., S. Aoufouchi, S. Weller, F. Vuillier, A. Stary, A. Sarasin, C.A. Reynaud, and J.C. Weill. 2004. DNA polymerase η is involved in hypermutation occurring during immunoglobulin class switch recombination. *J. Exp. Med.* 199:265–270.
50. Schrader, C.E., S.P. Bradley, J. Vardo, S.N. Mochegova, E. Flanagan, and J. Stavnezer. 2003. Mutations occur in the Ig S mu region but rarely in Sgamma regions prior to class switch recombination. *EMBO J.* 22:5893–5903.
51. Wittschieben, J.P., S.C. Reshmi, S.M. Gollin, and R.D. Wood. 2006. Loss of DNA polymerase zeta causes chromosomal instability in mammalian cells. *Cancer Res.* 66:134–142.
52. Sonoda, E., T. Okada, G.Y. Zhao, S. Tateishi, K. Araki, M. Yamaizumi, T. Yagi, N.S. Verkaik, D.C. van Gent, M. Takata, and S. Takeda. 2003. Multiple roles of Rev3, the catalytic subunit of polzeta in maintaining genome stability in vertebrates. *EMBO J.* 22:3188–3197.
53. Callen, E., M. Jankovic, S. Difilippantonio, J.A. Daniel, H.T. Chen, A. Celeste, M. Pellegrini, K. McBride, D. Wangsa, A.L. Bredemeyer, et al. 2007. ATM prevents the persistence and propagation of chromosome breaks in lymphocytes. *Cell*. 130:63–75.
54. Bemark, M., J.E. Sale, H.J. Kim, C. Berek, R.A. Cosgrove, and M.S. Neuberger. 2000. Somatic hypermutation in the absence of DNA-dependent protein kinase catalytic subunit (DNA-PK_{cs}) or recombination-activating gene (RAG)1 activity. *J. Exp. Med.* 192:1509–1514.
55. Delbos, F., S. Aoufouchi, A. Faili, J.C. Weill, and C.A. Reynaud. 2007. DNA polymerase η is the sole contributor of A/T modifications during immunoglobulin gene hypermutation in the mouse. *J. Exp. Med.* 204:17–23.
56. Schrader, C.E., J.E. Guikema, E.K. Linehan, E. Selsing, and J. Stavnezer. 2007. Activation-induced cytidine deaminase-dependent DNA breaks in class switch recombination occur during G1 phase of the cell cycle and depend upon mismatch repair. *J. Immunol.* 179:6064–6071.
57. Chen, X., K. Kinoshita, and T. Honjo. 2001. Variable deletion and duplication at recombination junction ends: implication for staggered double-strand cleavage in class-switch recombination. *Proc. Natl. Acad. Sci. USA*. 98:13860–13865.
58. Rush, J.S., S.D. Fugmann, and D.G. Schatz. 2004. Staggered AID-dependent DNA double strand breaks are the predominant DNA lesions targeted to S mu in Ig class switch recombination. *Int. Immunol.* 16:549–557.
59. Hirano, Y., and K. Sugimoto. 2006. ATR homolog Mec1 controls association of DNA polymerase zeta-Rev1 complex with regions near a double-strand break. *Curr. Biol.* 16:586–590.
60. Sabbioneda, S., I. Bortolomai, M. Giannattasio, P. Plevani, and M. Muzi-Falconi. 2007. Yeast Rev1 is cell cycle regulated, phosphorylated in response to DNA damage and its binding to chromosomes is dependent upon MEC1. *DNA Repair (Amst.)*. 6:121–127.
61. Mahajan, K.N., S.A. Nick McElhinny, B.S. Mitchell, and D.A. Ramsden. 2002. Association of DNA polymerase mu (pol mu) with Ku and ligase IV: role for pol mu in end-joining double-strand break repair. *Mol. Cell. Biol.* 22:5194–5202.
62. Fan, W., and X. Wu. 2004. DNA polymerase lambda can elongate on DNA substrates mimicking non-homologous end joining and interact with XRCC4-ligase IV complex. *Biochem. Biophys. Res. Commun.* 323:1328–1333.